Numerical study of soil collapse behavior by discrete element modelling

S.H. Liu[a,b,*], D.A. Sun[b], Yisen Wang[a]

[a]*Water Resources and Hydropower Planning and Design General Institute, MWR, Beijing, 100011, PR China*
[b]*Department of Civil Engineering, Nagoya Institute of Technology, Gokiso-cho, Showa-ku, Nagoya, 466-8555, Japan*

Abstract

In unsaturated granular soil, capillary suction produces an adhesive force that acts perpendicular to the tangential plane at each contact point. In this paper, the collapse behavior of unsaturated granular soil during isotropic compression and biaxial shear are numerically simulated using the distinct element method (DEM) by incorporating this adhesive force initially at all contacts and then releasing it continuously to zero. The simulated results are compared with the results of triaxial compression tests on unsaturated compacted clay and qualitative similarities are obtained. Based on the simulation results, the yield stresses under different interparticle adhesive forces are determined and the collapse processes before and after yielding are investigated in detail. Moreover, the effect of initial void ratio and principal stress ratio on collapse is also investigated and discussed. The paper illustrates the capacity of simulating qualitatively the collapse behavior of unsaturated granular soils through the changes of the interparticle adhesive forces produced by the capillary suction.
© 2003 Published by Elsevier Science Ltd.

Keywords: Capillary suction; Collapse; Distinct element method; Interparticle adhesive force; Unsaturated soil

1. Introduction

Volume decreases accompanying increases in water content at essentially unchanging total stresses in loose, partly saturated natural soil deposits have been termed collapse. Considerable experimental research has been conducted to study collapse of naturally deposited or artificially compacted soils [1,2] using both a conventional or double oedometer and a triaxial laboratory test. Several soil constitutive models [3–6] have been proposed for modeling the collapsing soil behavior. Through these studies, it has been revealed that the wetting-induced collapse is mainly due to the changes of the matric suction acting on the unsaturated soil structure. For unsaturated granular soils, the matric suction is considered to result essentially from the capillary action of the meniscus water surrounding the contacts between soil particles, which produce an interparticle adhesive force acting perpendicular to the contact plane of soil particles. Therefore, wetting-induced collapse is also considered to result from the changes of the interparticle adhesive forces. By incorporating an interparticle adhesive force in the specimen, Liu and Sun [7] proposed a numerical method for simulating the collapse of unsaturated granular soils by the distinct element method (DEM) [8]. In this paper, a biaxial compression test is simulated using this numerical method in order to study the collapse of unsaturated granular soils. The effects of interparticle adhesive force, initial void ratio and deviatoric stress are considered.

The numerical study of soil collapse by the DEM has some advantages over laboratory tests. For example, in laboratory tests on unsaturated soils, it's difficult to prepare soil specimens with different suction while keeping the other initial conditions identical. It is also difficult to measure accurately the volume change of the specimens due to the existence of pore air in unsaturated soil specimens. However, in DEM simulation, different interparticle adhesive forces (equivalent to matric suctions) can be incorporated in the specimen with the

* Corresponding author at: Nakata-so 7-503, Wakamizu 2-4-7 Chikusa-ku, Nagoya 464-0071, Japan. Tel.: +81-52-735-5497 or +81-52-722-4918; fax: +81-52-735-5497.
E-mail address: sihong@doboku2.ace.nitech.ac.jp (S.H. Liu).

same initial void ratio, and the volume change of the specimen can be correctly calculated.

2. Suction and interparticle adhesive force

Because water is attached to soil particles and it can develop surface tension, capillary menisci form between particles in a partially saturated soil mass. The curved air–water interface causes a pore water tension which, in turn, generates a suction s and an interparticle force P_s. If the soil particles are modeled as uniform spheres, then the generated suction s and interparticle force P_s can be calculated by the following equations (cf. Fig. 1):

$$\left.\begin{array}{l} s = u_a - u_w = T(1/r - 1/b) \\ P_s = (u_a - u_w)\pi b^2 + T(2\pi b) \end{array}\right\} \tag{1}$$

where u_a and u_w are the pore-air and pore-water pressures, respectively, T is the surface tension of the capillary water, and r and b are the radii of the meniscus and capillary water cylinder at its center. The radii, r and b, can further be expressed in terms of the radius R of the particle and the angle α of capillary water retention, using geometrical considerations, by Eqs. (2) and (3).

$$b = R(\tan\alpha + 1 - \sec\alpha) \tag{2}$$

$$r = R(\sec\alpha - 1) \tag{3}$$

The real soil particle has different shapes and may not be uniformly spherical as shown in Fig. 1, but the meniscus and its capillary action usually exist in a partially saturated soil when the degree of saturation is low, which induces an interparticle adhesive force. This force affects the mechanical behavior of partially saturated soil. In simulating the collapse phenomenon of an unsaturated granular material using DEM, an interparticle adhesive force is incorporated at particle con-

tacts in an initial DEM specimen and then released under a constant stress state.

It is usually considered that wetting-induced collapse occurs when the bonding or cementing agent in the partially saturated condition is reduced. From a micromechanical point of view, this bonding results from the interparticle adhesive force due to the water meniscus, and the bonding stress σ_s in the specimen can be estimated by Eq. (4) [9].

$$\sigma_s = \frac{2P_s}{\pi^2 R_m^2(1 + e)} \tag{4}$$

where R_m is the average radius of the particles along the mobilized plane and e is the void ratio of the specimen. This internal bonding stress σ_s is equivalent to the suction stress $\sigma_0(s)$ that is defined for unsaturated soils and is related to the suction s [5].

3. Biaxial compression test simulation

3.1. Outline of DEM analysis with an interparticle adhesive force

Only a brief introduction to the two-dimensional DEM is given here. The DEM is a numerical technique in which individual particles are represented as rigid bodies. In two dimensions, each particle has three degrees of freedom (two translations and one rotation). Each particle can be in contact with neighboring particles or structure boundaries. The contact between two particles, or a particle and a boundary, is modeled by a spring and dashpot in both the normal and tangential directions [see Fig. 2(b)]. The normal direction spring has a no-tension constraint. In the tangential direction, if the tangential force reaches a Coulomb friction limit, it is allowed to slide. Small amounts of viscous damping are often included to help provide dissipation of high-frequency motion. The forces generated at a contact are computed based on the overlap of the bodies at the contact and the stiffness of the springs.
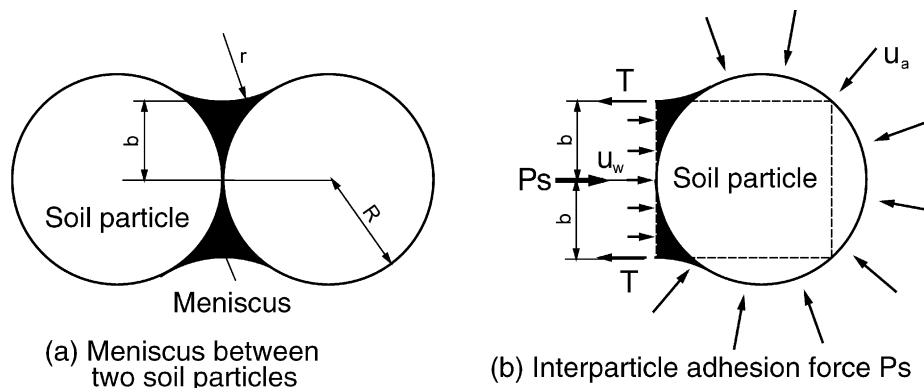

(a) Meniscus between two soil particles

(b) Interparticle adhesion force Ps

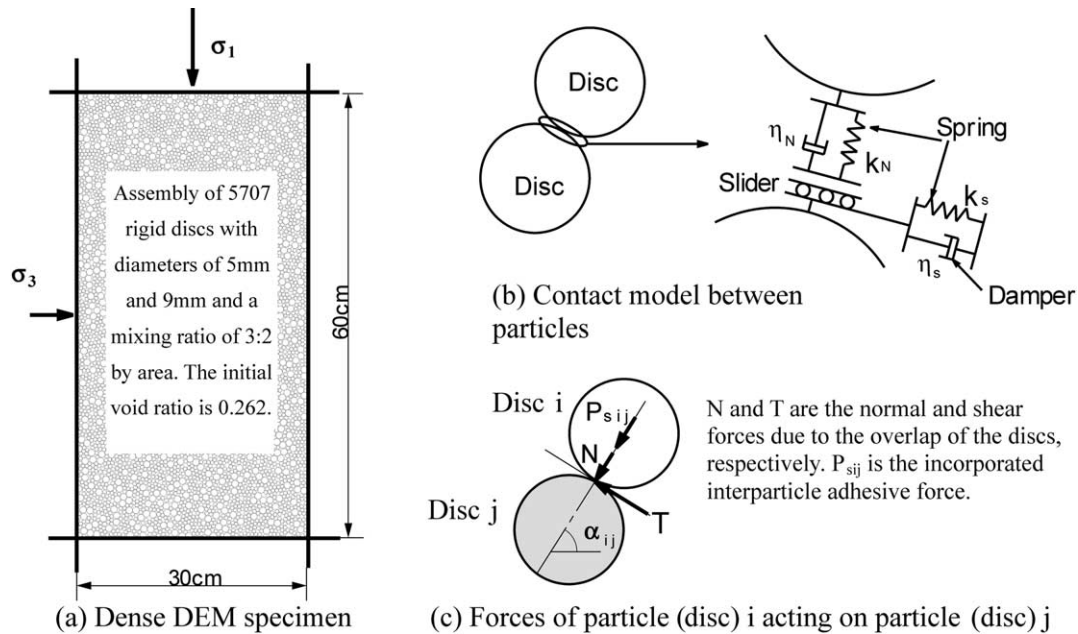Fig. 1. Interparticle adhesive force due to water menisus.

Fig. 2. DEM specimen and contact modelling.

In this study, the computer code used for the DEM is GRADIA, which was programmed by Yamamoto [10]. In order to account for the effect of suction in an unsaturated soil, we incorporate an interparticle adhesive force at contacts in GRADIA. The interparticle adhesive force that acts perpendicular to the contact plane between particles i and j is denoted as P_{sij} [see Fig. 2(c)]. The components of the resultant forces in the x and y directions, as well as the resultant moment acting on particle i due to P_{sij}, are given by the following equations:

$$
\left.\begin{aligned}
\left[F_{xi}^{p}\right]_{t} &= \sum_{j} P_{sij}\cos\alpha_{ij} \\
\left[F_{yi}^{p}\right]_{t} &= \sum_{j} P_{sij}\sin\alpha_{ij} \\
\left[M_{i}^{p}\right]_{t} &= 0
\end{aligned}\right\} \tag{5}
$$

where α_{ij} is the angle of the line connecting the centers of the contacting particles i and j to the x-axis. The force components due to the interparticle adhesive force P_{sij}, calculated from Eq. (5), are added to the forces based on the overlap of the bodies at the contact and the stiffness of the springs, yielding a final resultant force which is then used to compute the acceleration of the body according to Newton's laws of motion. After the acceleration is determined, new velocity and displacement for the particle is computed using central difference explicit time integration. To ensure convergence of the numerical solution, the time step Δt is taken to be $1/10\Delta t_c$, where Δt_c is the critical time step. The critical time step is estimated on the basis of a single degree-of-freedom system of a mass m connected to the ground by a spring of stiffness k, for which the critical

time step Δt_c equals $2\sqrt{m/k}$. With the newly computed displacement configuration, the state of deformation at the existing contacts is re-evaluated, and the possible creation of new contacts is allowed for, leading to a new cycle of computation.

3.2. Numerical simulation for biaxial compression tests

One of the objectives of this paper is to study the effect of initial void ratio of unsaturated granular soil on collapse. Thus, two rectangular DEM specimens consisting of two kinds of circular particles with diameters of 5 mm and 9 mm and a mixing ratio of 3:2 by area are generated. One specimen has an initial size of 60 cm by 30 cm and an initial void ratio of 0.262 [see Fig. 2(a)]; the other specimen has an initial size of 64.9 cm by 30 cm and an initial void ratio of 0.298. The specimens are bounded by four rigid walls, and the contacts between the particles and the rigid walls are modeled with springs and dashpots in both the normal and tangential directions. The input parameters used in our DEM simulation are summarized in Table 1. These parameters have been used to simulate biaxial compression, simple shear and direct shear tests on an assembly of aluminum rods with diameters of 5 mm and 9 mm and a mixing ratio of 3:2 by weight, and the simulated results agreed very well with the corresponding experimental results [10–12].

For a real unsaturated soil with a certain suction, the magnitude of the adhesive force P_s at each contact point between the soil particles may be different. They may differ due to the size and shape of soil particles as well as the pore water state inside soil voids and so on. In

Table 1
Input parameters for numerical simulation by DEM

	Particle–particle		Particle–platen
Normal stiffness k_N, k'_N (N/m/m)	5.0×10^9		9.0×10^9
Shear stiffness k_S, k'_S (N/m/m)	1.5×10^8		3.0×10^8
Normal damping η_N, η'_N (N s/m/m)	5.56×10^4		7.8×10^4
Shear damping η_S, η'_S (N s/m/m)	0.99×10^4		1.4×10^4
Interparticle friction angle ϕ_μ, ϕ'_μ (°)	16		16
Density of particles ρ (kg/m³)		2700	
Time increment Δt (s)		5×10^{-7}	

this study, a constant value of P_s is applied at each contact in the DEM specimen. This simple hypothesis will not model a real unsaturated soil exactly. It needs further study and development of the exact simulation for a real unsaturated soil.

In this study, five interparticle adhesive forces P_s of 5N, 9.8N, 14.7N, 19.6N and 49N are introduced at the contacts between particles for two initial specimens. These are, respectively, equivalent to internal bonding stresses σ_s of about 64.6 kPa, 126.6 kPa, 189.9 kPa, 253.2 kPa and 633.1 kPa as estimated by Eq. (4). These internal bonding stresses σ_s are within the ranges of the suction stresses commonly applied to unsaturated soil specimens in laboratory experiments [5]. Each specimen is isotropically compressed under increasing mean stress $p = (\sigma_1 + \sigma_3)/2$ ($\sigma_2 = 0$ for biaxial compression). At such the previously specified mean stresses that are extremely low (about 1kPa), near and after the yield stresses, the incorporated interparticle adhesive force is released gradually to zero to simulate the collapse phenomenon of unsaturated soil during compression. Then, the specimens with $P_s = 9.8$N are sheared at a constant mean stress $p = 196$ kPa. At several constant deviatoric stresses, the interparticle adhesive forces incorporated in the specimens are released gradually to zero to simulate the collapse phenomenon of unsaturated soil during shear.

In our simulation, the specimen is loaded in a stress-controlled way. At every stress increment, the calculation is continued until all the particles and the boundary rigid walls move with accelerations less than $0.5g$ (g = gravity acceleration). The volume change and strains of the specimen are calculated from the displacements of the four rigid boundary walls.

4. Numerical results and comparisons with experimental results on unsaturated compacted clay

4.1. Simulated yield curves of unsaturated granular soil

Fig. 3 shows the numerically simulated e–$\ln p$ compression curves during isotropic compression in the cases of $P_s = 9.8$N, 14.7N, 19.6N and 49N. Clearly, under a constant interparticle adhesive force P_s, there

exists a yield stress, p_y, which is determined approximately to be the stress at the inflexion point as illustrated in Fig. 3(b). It can be seen that the yield stress p_y increases with increasing interparticle adhesive force P_s and decreasing void ratio e (the specimen becomes denser).

From a microscopic point of view, the interparticle adhesive force P_s due to capillary action contributes to the shearing resistance of grains. For unsaturated soils, the shear and normal contact forces, f_s and f_n, at any typical contact point are caused by both external and interparticle adhesive forces [see Fig. 2(c)], expressed as

$$f_s = T, \quad f_n = N + P_s \tag{6}$$

where N and T are, respectively, the normal and shear forces caused by external loading. The maximum possible shear resistance T_{max} at grain contact points will be

$$T_{max} = f_n \tan\phi_\mu = N \tan\phi_\mu + P_s \tan\phi_\mu \tag{7}$$

where ϕ_μ is the angle of friction between soil particles. The second term in Eq. (7), denoted as $c_s = P_s \tan\phi_\mu$, is regarded as a nominal cohesion [13]. Obviously, the nominal cohesion c_s becomes large when P_s increases, which thereby increases the resistance to the grain slippage. Therefore, the yield stress p_y where the soil begins plastic deformation due to grain slippage is large at high P_s.

Fig. 4 gives the P_s versus p_y relations (yield curves) determined from Fig. 3 (the e–$\ln p$ compression curves in the case of $P_s = 5$N are not presented in Fig. 3). As expected, it is seen from Fig. 4 that the yield limit enlarges when the specimen becomes denser (the initial void ratio decreases). If the DEM specimen is extremely loose, then the yield limits might pass through the origin, i.e. the yield stress $p_y = 0$ when $P_s = 0$N. But, because the initial DEM specimens that are simulated in this study are not in the loosest states, it is deduced that the yield curves as illustrated in Fig. 4 may not pass through the origin. As known from Eq. (1), the interparticle adhesive force P_s is closely related to suction, thus these simulated yield curves have meanings which are similar to the loading collapse yield curves as proposed by many researchers [4–6].
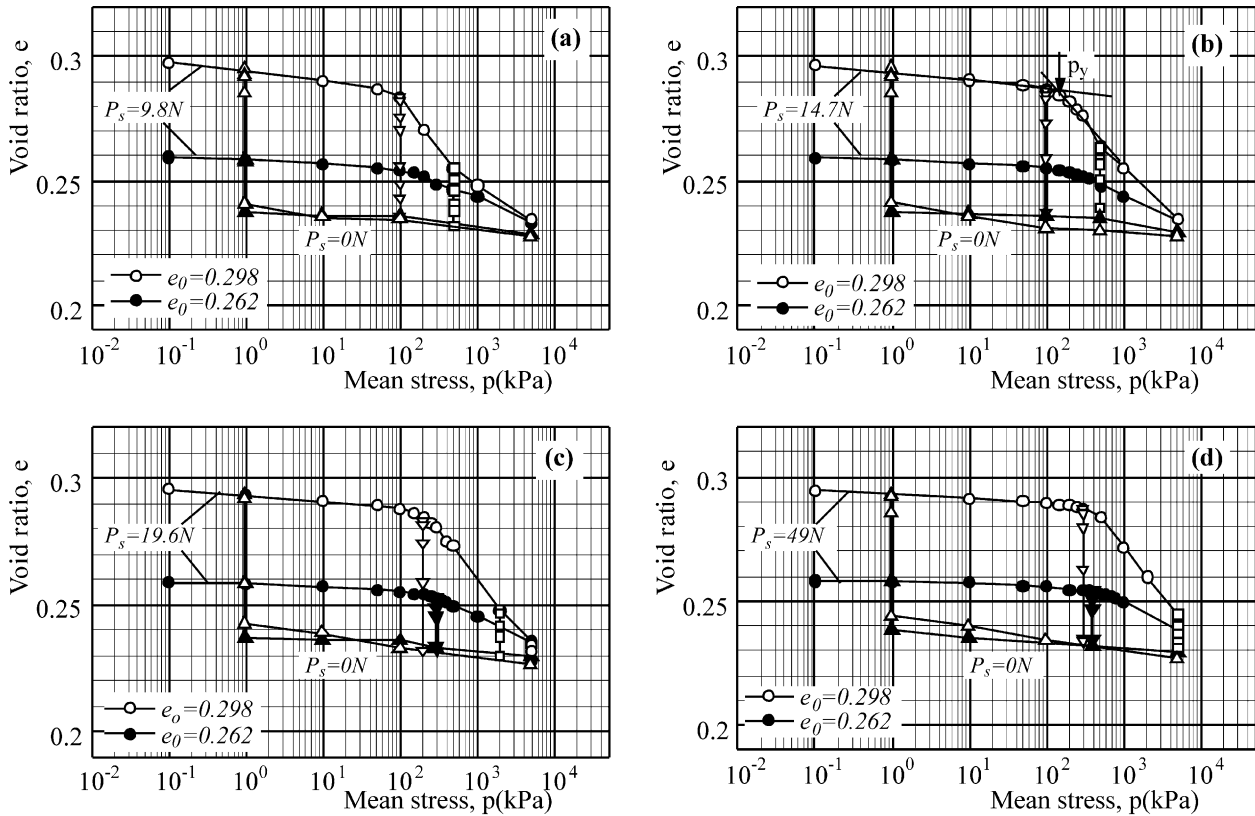
Fig. 3. Volume change of numerically simulated biaxial compression tests during isotropic compression.

4.2. Volume changes under isotropic compression

Fig. 3 also gives the collapse deformations simulated under several constant mean stresses. As stated in Section 3.2, the collapse of unsaturated soil during isotropic compression is simulated by releasing the interparticle adhesive forces P_s in several steps from their initial values to zero. In the case where the interparticle adhesive force P_s is released from the incorpo-

Fig. 4. Yield stresses plotted against interparticle adhesive forces corresponding to Fig. 3.

rated value to zero at constant mean stress $p = 1$ kPa, the specimens are continuously compressed to $p = 5$ MPa.

Fig. 5 shows the laboratory experimental results of unsaturated compacted pearl clay at two different initial void ratios ($e_0 = 1.36$ and 1.27) [14,15]. The laboratory tests were conducted in an improved triaxial cell for controlling suction by adopting the axis translation technique and measuring directly the lateral strain of specimens with two bronze rings. All the triaxial specimens, 3.5 cm in diameter and 8.0 cm high, were prepared identically by compaction in a mould in five layers, and each layer was statically compacted 10 times using a 1.2 cm plunger up to a vertical stress of 314 kPa. The compacted specimens had a dry density of about 1.15 g/cm³, an initial degree of saturation of about 50%, and an initial matric suction of about 100 kPa. At the beginning of the tests, the specimens with the initial suction of about 100 kPa were first consolidated at a total mean stress of 20 kPa, and then a specific air pressure was applied to the specimens until the matric suction of the specimens achieved a constant value of 147 kPa. After that, the specimens were isotropically compressed under a constant matric suction of 147 kPa. During isotropic compression, the matric suction in the specimens was reduced in several steps from 147 kPa to 0 kPa, at some previously specified net confining pressure, to cause the collapse deformation. Comparison of
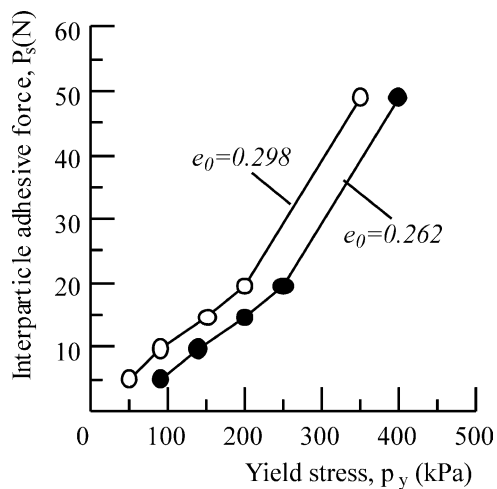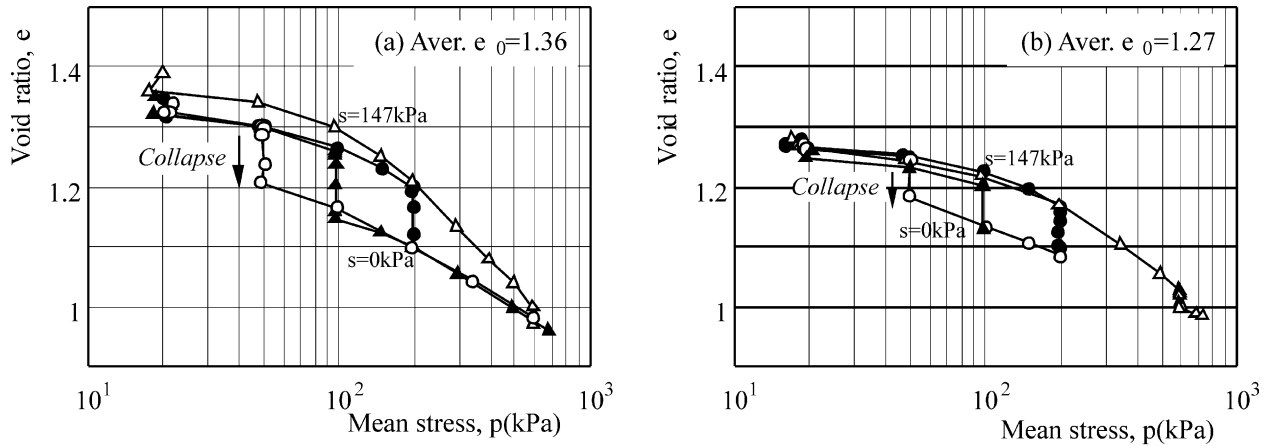
Fig. 5. Volume change of compacted pearl-clay under isotropic compression with wetting (after [14,15]).

Fig. 3 with Fig. 5 shows that there are qualitative similarities between the numerical and experimental results, indicating the usefulness of the proposed numerical modeling method.

From Figs. 3 and 5, the following collapse behavior for unsaturated soils under isotropic compression can be observed:

1. The volume change (collapse deformation), induced by releasing the interparticle adhesive force P_s, varies with the applied mean stress p. The compression curves (the void ratios plotted against mean stresses p) after collapse are closely arranged on the same compression curve as that obtained from the subsequent compression when the incorporated P_s is released to zero under conditions of constant mean stress $p = 1$ kPa. For a specimen with a specified constant P_s, the collapse deformation is small at lower and higher mean stresses p, and the largest near the yield stress p_y. Fig. 3 also suggests that the magnitude of the collapse deformation increases with increasing P_s. This is because the higher P_s induces lower compressibility of the specimen due to the larger resistance to grain slippage.

2. The initial void ratio of the specimen affects the magnitudes of the volume changes (collapse) that are induced by releasing the interparticle adhesive force P_s. At the same applied mean stress, the collapse in a loose specimen is larger than that in a dense specimen. However, it seems that the compression curves after collapse are identical, irrespective of the initial void ratios, which would probably be useful for constructing a constitutive model to predict soil collapse. This needs further experimental investigation.

Microscopic investigations of the DEM specimens have shown that the particle contacts increase with iso-

tropic compression and following the collapse induced by releasing the interparticle adhesive force P_s. An example of the average co-ordination number plotted against mean stress is illustrated in Fig. 6, which corresponds to the specimens with an initial value of $P_s = 19.6$N. The average co-ordination number is defined as M/N, where M is twice the number of physical contacts and N is the number of particles [16]. Apparently, the average co-ordination number increases with increasing mean stress both in dense and loose specimens. For the example shown in Fig. 6, the average co-ordination number is larger in the dense specimen ($e_0 = 0.262$) than in the loose specimen ($e_0 = 0.298$) when the mean stress $p < 100$ kPa, and tends to be identical when the mean stress $p > 100$ kPa. This may suggest that, at lower mean stresses, the different magnitudes of volume changes in dense and loose specimens result from both the particle rearrangement and the slippage between particles, while at high mean stresses, they are caused mainly by the different slippage between particles. In Fig. 6, we see that the average co-ordination
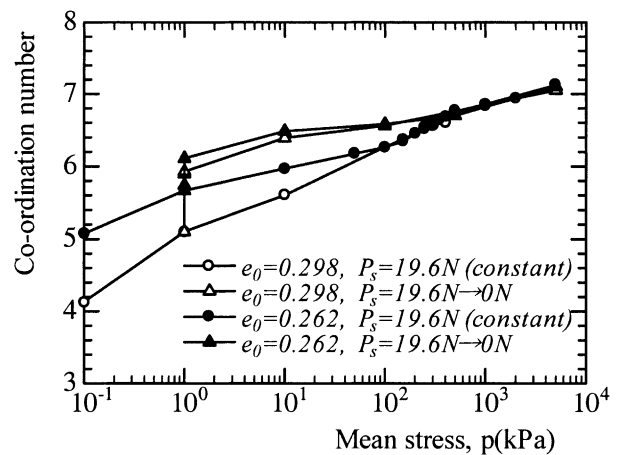

Fig. 6. Evolution of co-ordination number during isotropic compression and release of P_s.

number increases when collapse occurs under constant mean stress $p = 1$ kPa, and this increase is larger in the loose specimen than in the dense specimen. However, during the subsequently isotropic compression after collapse, the development of the average co-ordination number is almost the same in both the dense and the loose specimens.

We now investigate the volume change of the specimens when the interparticle forces P_s are released under conditions of constant mean stress p, i.e. the collapse process following the release of P_s. Here, we define the collapse volumetric strain as $\varepsilon_v = -\Delta e/(1 + e_b)$, where e_b is the initial void ratio and Δe is the difference of the void ratio after and before the release in P_s. ϵ_v is taken positive for specimen compression. The evolution of the collapse volumetric strains during the collapse process for the loose specimens ($e_0 = 0.298$) with the initially incorporated values of $P_s = 9.8$N, 14.7N, 19.6N and 49N are illustrated in Fig. 7. It can be seen that the collapse process varies with the magnitude of the mean stress p. At low mean stress ($p = 1$ kPa in Fig. 7), the collapse volumetric strains are very small or even negative (the volume of the specimens expand) as P_s is initially released and increase rapidly at the end of the

process. For example, under conditions of constant $p = 1$ kPa in Fig. 7(a), the volume of the specimen expands slightly ($\varepsilon_v < 0$) when P_s is released from the initial value of 9.8 to 5 N, and then subsequently contracts when P_s is released further. During the final stage of releasing P_s from 1 N to 0 N, the collapse volumetric strain increases rapidly. The small compressibility due to a release in the interparticle forces P_s (equivalent to a change in matric suction) at low mean stress p is considered to result from elastic compression without grain slippage (cf. Fig. 4), whereas the rapid increase in collapse deformation at the final stage of releasing P_s (at low mean stress p) might result from the failure of the metastable structure in unsaturated soils due to structural rearrangement. This argument may be supported by the fact that the average co-ordination number increases slightly at the initial stage of releasing P_s and increases rapidly at the final stage of releasing P_s, as illustrated in Fig. 6. At high mean stresses p (near or higher than the yield stresses p_y), e.g. $p = 98$ kPa and 490 kPa in Fig. 7(a), the collapse volumetric strains increase almost in a monotonic way as the interparticle forces P_s are released. This is because at high mean stresses p, near or higher than the yield stresses p_y, the collapse
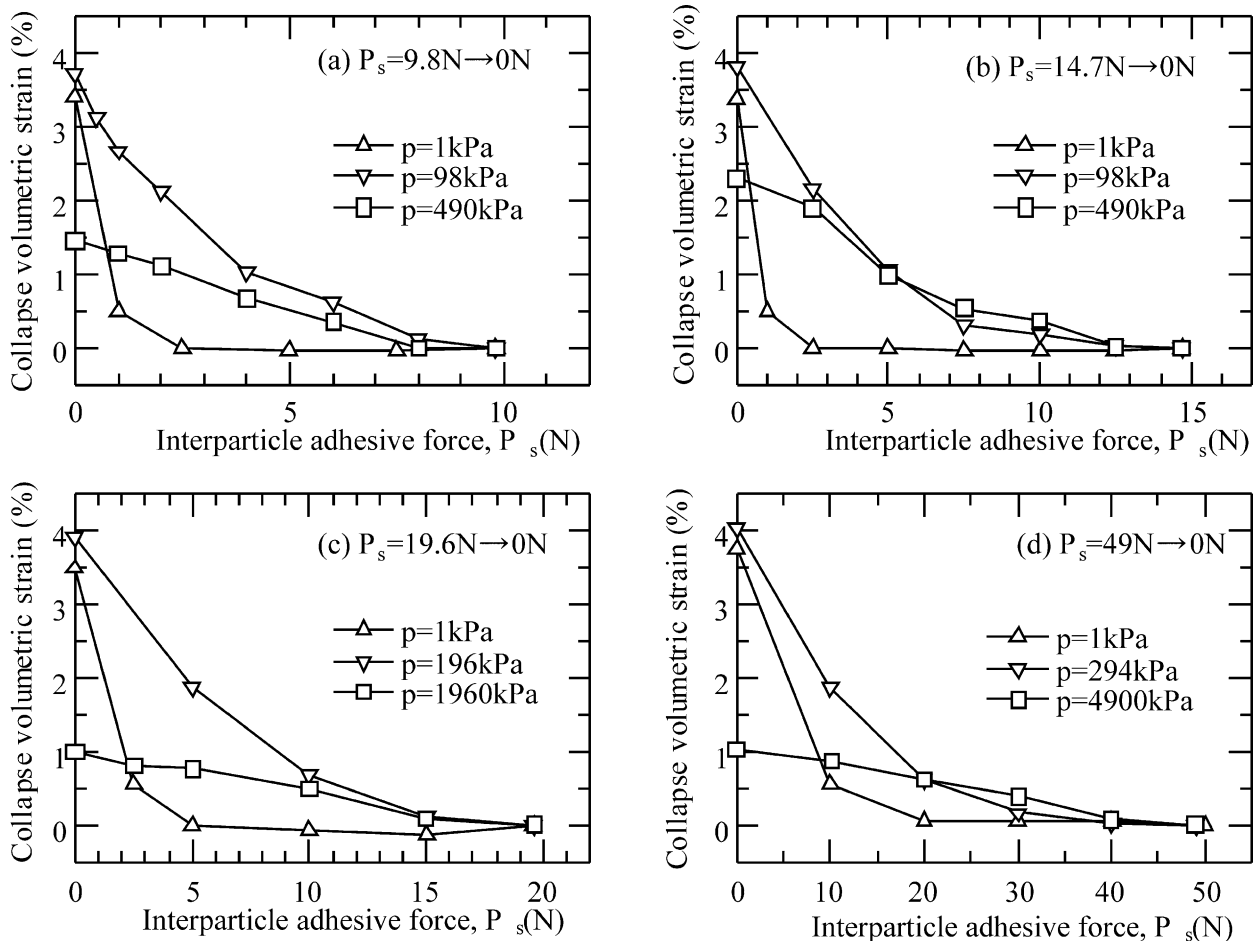

Fig. 7. Collapse process under conditions of different constant mean stresses for the specimen with initial void ratio $e_0 = 0.298$.

deformation involves both elastic and plastic compression from the beginning of releasing P_s (cf. Fig. 4). Fig. 8 shows the collapse process behavior analyzed by using the experimental data in Fig. 5(a). The comparison of Fig. 8 with Fig. 7 shows that the numerically simulated collapse behavior, under conditions of different constant mean stress, are in qualitative agreement with the experimental results.

4.3. Collapse behavior during shear

The collapse during shear is simulated by means of releasing the incorporated interparticle force P_s under conditions of constant principal stress ratio. The effects of initial void ratio and principal stress ratio on the collapse behavior are investigated.

Figs. 9 shows the stress–strain relationships of the numerically simulated biaxial compression tests on the two samples with different initial void ratios, in which (a) the initially incorporated $P_s = 9.8$ N is released to zero under conditions of constant $\sigma_1/\sigma_3 = 1.3$ and (b) the initially incorporated $P_s = 9.8$ N is released to zero under conditions of constant $\sigma_1/\sigma_3 = 1.5$. It can be seen that the magnitudes of both the volumetric collapsing strain, ε_v, and the vertical collapsing strain, ε_1, caused

Fig. 8. Collapse process of compacted pearl-clay under constant mean stresses p corresponding to Fig. 5(a) (after [14]).

by releasing P_s in the loose specimen ($e_0 = 0.298$) are larger than those in the dense specimen ($e_0 = 0.262$), irrespective of the principal stress ratio. At the beginning of the release of the interparticle force P_s, the specimens contract slightly in the lateral direction until the expansion due to the applied deviatoric stress balances the contraction due to the internal confinement of P_s. This phenomenon is obvious in the dense specimen when releasing P_s under low constant principal stress ratio ($\sigma_1/\sigma_3 = 1.3$), as illustrated in Fig. 9(a). For the specimens with an initial void ratio of 0.262, the simulated stress–strain responses with P_s released under $\sigma_1/\sigma_3 = 1.3$ and 1.5 are summarized in Fig. 10, together with the simulated results in the case of $P_s = 0$. It can be seen that the magnitude of the vertical collapsing strain ε_1 (compression), caused by releasing P_s, increases and the magnitude of the lateral collapsing strain ε_3 (extension) decreases, with increasing principal stress ratio. The strain-stress responses after releasing P_s from 9.8N to zero, however, tend to be the same and nearly coincide with those in the case of $P_s = 0$. This behavior is similar to the experimental results on unsaturated compacted Pearl-clay shown in Fig. 11 [15].

During shearing deformation, the contacts oriented along the direction of maximum tensile strain disintegrate more rapidly than the contacts in other directions. Consequently, the distribution of the contact orientations becomes anisotropic. This stress-induced anisotropy in contact orientations can be best described in terms of the ratio of the principal values, F_{11}/F_{22}, of the second-order fabric tensor, F_{ij}, that was proposed by Satake [17] and expressed as

$$F_{ij} = \frac{1}{2N} \sum_{k}^{2N} n_i^k n_j^k \qquad (8)$$

where N is the total number of contact points and $n_i^k (i = 1, 2)$ are the direction cosines of the unit vector $\boldsymbol{n}^k$ of the contact plane with respect to the reference axes x_i ($i = 1,2$). Fig. 12 shows the evolution of F_{11}/F_{22} plotted against the principal stress ratio σ_1/σ_3 for the specimens that are sheared under constant $P_s = 9.8$ N (denoted by AB lines), and for the specimens for which the initially

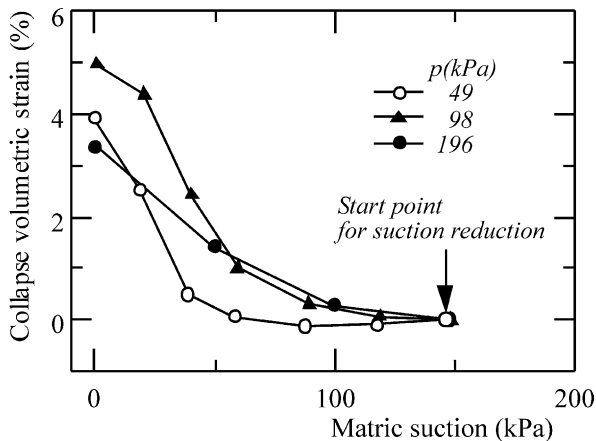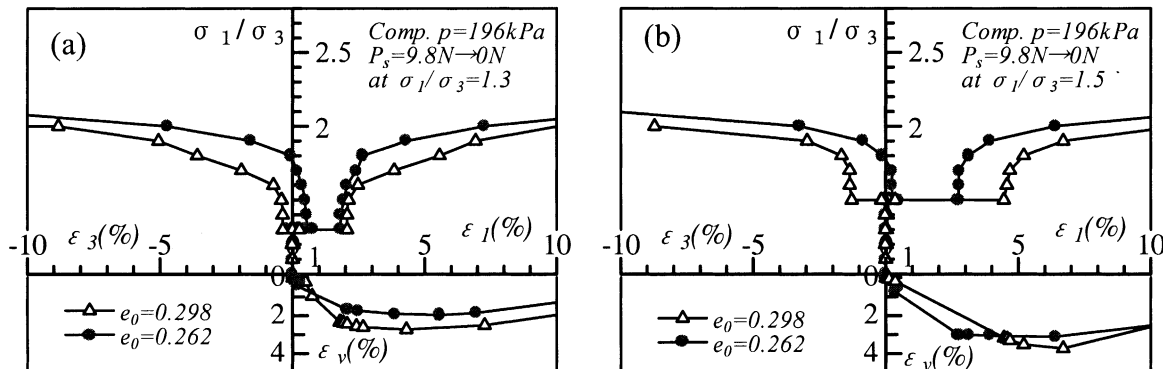Fig. 9. Effect of the initial void ratios on collapse behaviors during shear, releasing P_s under conditions of (a) $\sigma_1/\sigma_3 = 1.3$ and (b) $\sigma_1/\sigma_3 = 1.5$.

incorporated value of $P_s = 9.8$ N is released under conditions of $\sigma_1/\sigma_3 = 1.3$ and 1.5. Firstly, it is seen that the release in the interparticle adhesive force P_s causes an increase in F_{11}/F_{22}. The same values of F_{11}/F_{22} at points b′ and d in Fig. 12(a) suggest that the evolution of the fabric anisotropy accompanying a release in P_s (collapse) coincides with that for soils under shear. Thus,
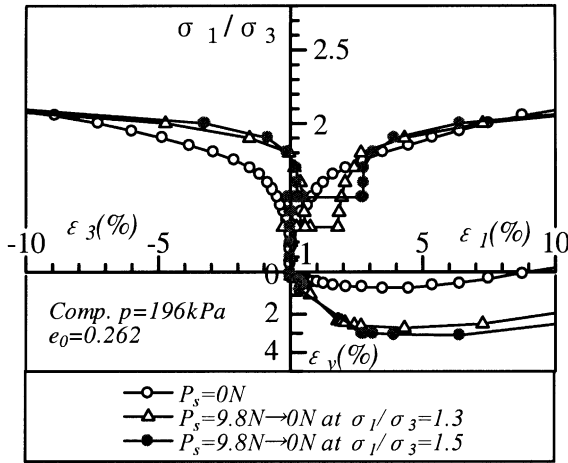
collapse during shear may be interpreted as a shear phenomenon. Moreover, it is seen from Fig. 12 that the increase in F_{11}/F_{22} due to a release in P_s at high σ_1/σ_3 is larger than that at low σ_1/σ_3 (e.g. $bb' > aa'$, $dd' > cc'$).

We now consider why the fabric anisotropy F_{11}/F_{22} increases as P_s is released. Satake [18] derived a relationship between the fabric anisotropy and the macroscopic stresses imposed on the assembly of granular materials, which is expressed as

$$\frac{F_{11}}{F_{22}} = \sqrt{\frac{\sigma_1 + p_0}{\sigma_3 + p_0}} \tag{9}$$

where p_0 $(= c \, cot\phi)$ is called the inherent cohesion. In fact, the bonding stress σ_s induced by the interparticle adhesive force P_s, as estimated by Eq. (4), is equivalent to this inherent cohesion p_0. Thus, the release in P_s is equivalent to the reduction of p_0 in the right side of Eq. (9), which thereafter causes the increase in the fabric anisotropy F_{11}/F_{22} while σ_1 and σ_3 are kept constant. For example, for the simulated specimen with $e = 0.262$, the bonding stress $\sigma_s = 128.5$ kPa with $P_s = 9.8$ N. According to Eq. (9), the fabric anisotropy F_{11}/F_{22} increases from 1.083 to 1.140 under the conditions of $p = 196$ kPa and $\sigma_1/\sigma_3 = 1.3$, and increases from 1.130 to 1.225 under the conditions of $p = 196$ kPa and

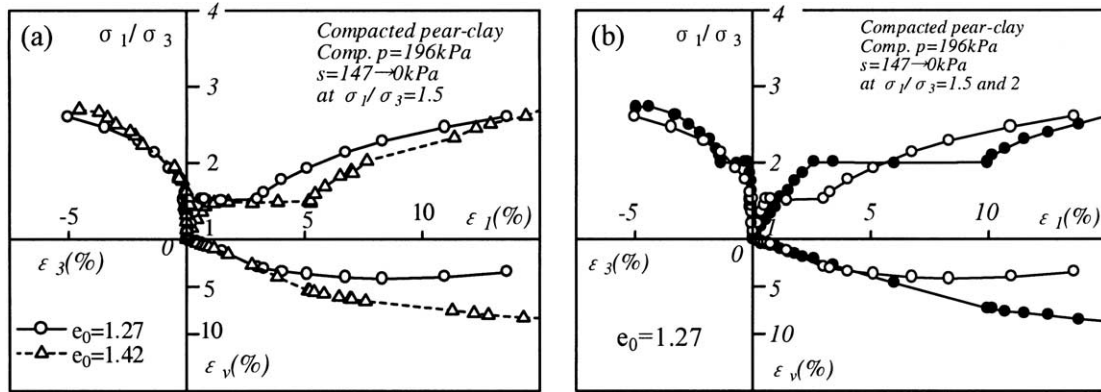Fig. 10. Effect of principal stress ratio on collapse behaviors during shear.

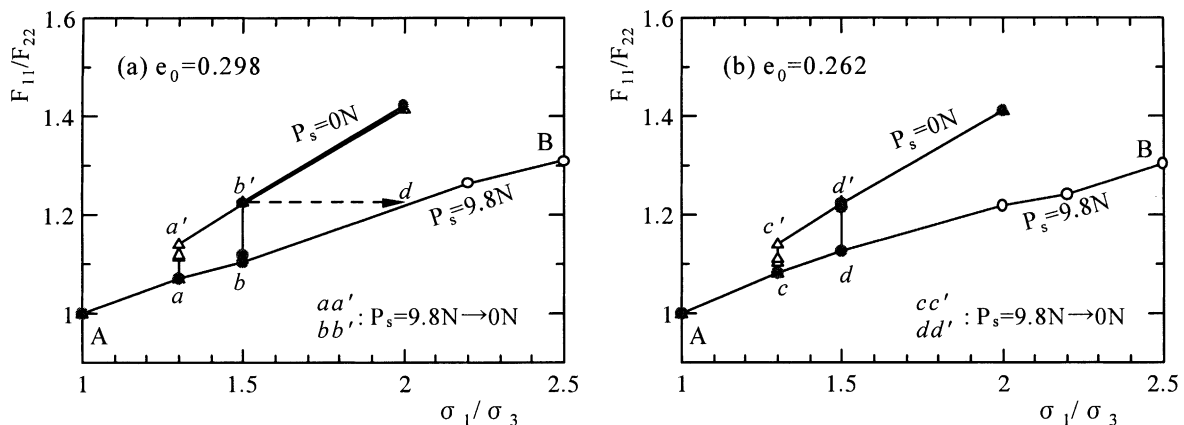Fig. 11. Results of triaxial compression tests on compacted Pearl-clay (after [15]).

Fig. 12. Induced anisotropy during shear accompanying with the release in interparticle adhesive force P_s under constant principal stress ratios.

$\sigma_1/\sigma_3 = 1.5$, respectively, when P_s is released from 9.8N to 0N. Eq. (9) implies that the slope of the line of F_{11}/F_{22} plotted against σ_1/σ_3 in Fig. 12 is larger for the specimens with $P_s = 0$N (after collapse) than that for the specimens with $P_s = 9.8$N.

5. Concluding remarks

A numerical model for simulating the collapse behavior of granular materials by the DEM has been presented in this paper. In this numerical model, the capillary suction in unsaturated soils is modeled with an interparticle adhesive force P_s that is initially incorporated at all contacts. Wetting-induced collapse is simulated by means of releasing the incorporated P_s. By using this numerical method, a biaxial compression test on assemblies of circular rigid particles has been simulated. The simulation results agree qualitatively with the results of triaxial compression tests on unsaturated compacted clay. The numerically simulated collapse behavior of granular materials may be summarized as follows:

1. During isotropic compression, the volume change (collapse deformation) induced by releasing the interparticle adhesive force P_s varies with the applied mean stress p, the incorporated P_s, and the initial void ratio e_0. However, the compression curves after completely releasing P_s under different mean stresses p are closely arranged on a unique line, irrespective of the initial void ratio e_0 (cf. Fig. 3). The evolution of the collapse deformation following a release in the interparticle adhesive forces P_s (i.e. the collapse process) is a function of the mean stress p (cf. Fig. 7). The collapse behavior during isotropic compression correlate microscopically with the changes in the average co-ordination number.

2. During biaxial shear, the collapse deformation caused by releasing P_s is affected by the initial void ratio and the principal stress ratio. For a specified interparticle adhesive force P_s, the magnitude of the vertical collapse strain ε_1 (compression) increases and the magnitude of the lateral collapsing strain ϵ_3 (extension) decreases with an increasing principal stress ratio. This effect is more obvious in loose specimens than in dense specimens. From a microscopic point of view, the release in the interparticle adhesive force P_s under the conditions of constant principal stress ratio induces an increase in the fabric aniso-

tropy defined by F_{11}/F_{22}. Thus, collapse during shear may be interpreted as a shear phenomenon.

References

[1] Lawton EC, Richard J, Fragaszy RJ, Hetherington MD. Review of wetting-induced collapse in compacted soil. Journal of Geotechnical Engineering, ASCE 1992;118(9):1376–94.

[2] Pereira JHF, Fredlund DG. Volume change behavior of collapsible compacted gneiss soil. Journal of Geotechnical and Geoenvironmental Engineering, ASCE 2000;126(10):907–16.

[3] Fredlund DG, Morgenstern NR. Constitutive relations for volume change in unsaturated soils. Canadian Geotechnical Journal 1976;13(3):261–76.

[4] Alonso FE, Gens A, Josa A. A constitutive model for partially saturated soils. Geotechnique 1990;40:405–30.

[5] Sun DA, Matsuoka H, Yao YP, Ichihara W. An elastoplastic model for unsaturated soil in three-dimensional stresses. Soils and Foundations 2000;40(3):17–28.

[6] Cui YJ, Yahia-Aissa M, Delage P. A model for the volume change behavior of heavily compacted swelling clays. Engineering Geology 2002;64:233–50.

[7] Liu SH, Sun DA. Simulating the collapse of unsaturated soil by DEM. Int J Numer Anal Mech Geomech 2002;26:633–46.

[8] Cundall PA, Strack ODL. A discrete numerical model for granular assemblies. Geotechnique 1979;29(1):47–65.

[9] Tateyama K, Fukui Y. Understanding of some behaviour of unsaturated soil by theoretical study on capillary action. In: Rahardjo Toll, Leong, editors. Proceeding of unsaturated soils for Asia. Rotterdam: Balkema; 2000. p. 163–8.

[10] Yamamoto S. Fundamental study on mechanical behavior of granular materials by DEM. Dr Eng thesis, Nagoya Institute of Technology, Japan, 1995 [in Japanese].

[11] Liu SH, Matsuoka H. A microscopic study on stress-dilatancy relationship of granular materials by DEM. Powers and Grains 2001:207–11.

[12] Liu SH. Development of a new direct shear test and its application to the problems of slope stability and bearing capacity. Dr Eng thesis, Nagoya Institute of Technology, Japan, 1999.

[13] Kohgo Y, Nakano M, Miyazaki T. Theoretical aspects of constitutive modeling for unsaturated soils. Soils and Foundations 1993;33(4):49–63.

[14] Sun DA, Xu YF, Matsuoka H. Collapse of compacted clays using triaxial test. In: Proceeding of 3rd Int. Conf. on unsaturated soils, vol. 2, 2002. p. 631–4.

[15] Sun DA, Matsuoka H, Xu YF. Effect of initial void ratio on collapse of compacted clay. In: Proceedings of the 57th Annual Conf. of JSCE, vol. III-335, 2002. p. 669–70.

[16] Rothenburg L, Bathurst RJ. Analytical study of induced anisotropy in idealized granular materials. Geotechnique 1989;39(4):601–14.

[17] Satake M. Constitution of mechanics of granular materials through the graph theory. In: Jenkins, Satake, M, editors. Proceeding of US-Japan Seminar on Continuum-mechanical and Statistical Approaches in the Mechanics of Granular Materials, Tokyo 1978, p. 9–19.

[18] Satake M. On induced anisotropy in granular materials. In: Proceedings of 28th Japan National Conf. on SMFE, 1993. p. 213–4 [in Japanese].